INTERNATIONAL JOURNAL FOR NUMERICAL METHODS IN FLUIDS, VOL. 25, 645–658 (1997)

NUMERICAL SIMULATION OF THREE-DIMENSIONAL FREE SURFACE FLOW IN ISOPYCNAL CO-ORDINATES

VINCENZO CASULLI*

Department of Civil and Environmental Engineering, University of Trento, I-38050 Mesiano di Povo (Trento), Italy and CIRM-ITC, I-38050 Povo (Trento), Italy

SUMMARY

In this paper a semi-implicit method for three-dimensional circulation in isopycnal co-ordinates is derived and discussed. It is assumed that the flow is hydrostatic and characterized by isopycnal surfaces which can be represented by explicit, single-valued functions. The hydrostatic pressure is determined by using the conjugate gradient method to solve a block pentadiagonal linear system. The horizontal velocities are determined by solving a large set of tridiagonal systems. The stability of the resulting algorithm is shown to be independent of the surface and internal gravity wave speeds. © 1997 John Wiley & Sons, Ltd.

Int. J. Numer. Meth. Fluids, **25**: 645–658 (1997)

No. of Figures: 10. No. of Tables: 0. No. of References: 13.

KEY WORDS: isopycnal model; semi-implicit method; hydrostatic approximation; internal waves; baroclinic flow; free surface

1. INTRODUCTION

A characteristic analysis of the two-dimensional, vertically integrated shallow water equations shows that the celerity term $\sqrt{(gH)}$ in the equation for the characteristic cone arises from the barotropic pressure gradient in the momentum equations and from the velocity derivatives in the free surface equation.[1] Results of this analysis have led to a practical semi-implicit method which has been proved to be stable and which has been extended to the three-dimensional equations where the pressure is assumed to be in hydrostatic equilibrium.[2] The Courant–Friedrichs–Lewy (CFL) stability condition relating the time step to the free surface wave speed is not required, because the barotropic pressure gradient in the momentum equations and the velocities in the vertically integrated continuity equation are finite-differenced implicitly.

Three-dimensional applications of the above semi-implicit scheme to lakes, estuaries and coastal seas have confirmed that this algorithm is stable and highly efficient (see e.g. Reference 2). Moreover, when only one vertical layer is specified, this method reduces to the semi-implicit method for the two-dimensional, vertically integrated shallow water equations as described in Reference 1 (see also Reference 3 for further details). The resulting two- and three-dimensional methods, however, are only first-order-accurate in time and often introduce unacceptable artificial damping.

* Correspondence to: V. Casulli, Department of Civil and Environmental Engineering, University of Trento, I-38050 Mesiano di Povo (Trento), Italy

CCC 0271–2091/97/060645–14 $17.50

Received August 1996
Revised October 1996

The stability, accuracy and efficiency of this three-dimensional algorithm have been studied in Reference 4, where the method has been further generalized by introducing an implicitness parameter θ. When $\theta = 1$, this method reverts to the semi-implicit scheme proposed in Reference 2. When $\theta = \frac{1}{2}$, the pressure gradient in the momentum equations and the velocities in the free surface equation are evaluated as an average of their values at time levels n and $n+1$, so that the discretization of these terms is second-order-accurate in time. Since the vertical viscosity terms have been discretized implicitly, it is proved that for $\frac{1}{2} \leqslant \theta \leqslant 1$ a mild stability condition is required on the time step which is related only to the horizontal discretization increments Δx and Δy through the horizontal viscosity coefficient. The three-dimensional simulation of baroclinic flows can be obtained in a direct way by including the baroclinic pressure terms in the horizontal momentum equations. These terms are coupled, through an equation of state, to a convection–diffusion equation for each conserved quantity such as salt, temperature and/or concentration of suspended sediment. The explicit treatment of the baroclinic pressure terms adds an additional stability restriction which relates the time step to the speed of internal waves. Nevertheless, an efficient and robust implementation of such a simple and reliable numerical method has resulted in a code (TRIM-3D) capable of handling two- and three-dimensional problems with extremely fine spatial resolution and relatively large time steps.

In this paper a semi-implicit isopycnal circulation model is presented as an alternative to traditional three-dimensional models in Cartesian (x, y, z) co-ordinates. The present formulation can be regarded as being three-dimensional in (x, y, ρ) co-ordinates and is better suited for studying stably stratified baroclinic circulation. Numerically, the new internal and external free surface locations are computed in a similar fashion as in Reference 1 by using the conjugate gradient method to solve a block pentadiagonal linear system. The horizontal velocity in each isopycnal layer is then determined by solving a large set of small tridiagonal systems. The stability of the resulting algorithm is shown to be independent of the surface and internal wave speeds. The convective and viscous terms in the momentum equations are conveniently discretized using a Eulerian–Lagrangian approach. The resulting algorithm conserves mass and volume and applies to simulations of complex three-dimensional baroclinic flows using fine spatial resolution and relatively large time steps. Neither artificial diffusion nor spurious oscillations are generated. This formulation is fully vectorizable and accounts naturally for vanishing layer thickness.

In the next section the governing equations of a three-dimensional isopycnal flow are introduced along with the corresponding boundary conditions at the layer interfaces. In Section 3 the basic semi-implicit finite difference discretization is given for the governing equations and for the corresponding boundary conditions. Section 4 discusses a practical solution algorithm which enables an efficient implementation of the method. A linearized stability analysis of the present method is outlined in Section 5. The essential properties of the model are summarized in Section 6 and, finally, in Section 7 the numerical results from two different test cases are presented and discussed.

2. GOVERNING EQUATIONS

Assuming stable stratification, the fluid density is monotonic increasing downwards. If density is conserved, as is approximately the case for most geophysical flows, considerable mathematical simplifications follow from considering the three-dimensional governing equations expressed in terms of density ρ rather than the vertical z-co-ordinate.[5] A layered isopycnal model is an ideal fluid system that consists of a finite number of moving layers stacked one upon another and each having a uniform density. For a system of M layers with densities $\rho_1 > \rho_2 > \cdots > \rho_M > 0$, let $z = \eta_k(x, y, t)$ be the surface of separation between layer k and the layer above $k+1$. The surfaces $z = \eta_0(x, y)$ and $z = \eta_M(x, y, t)$ represent the fixed bottom and the free surface respectively (see Figure 1).

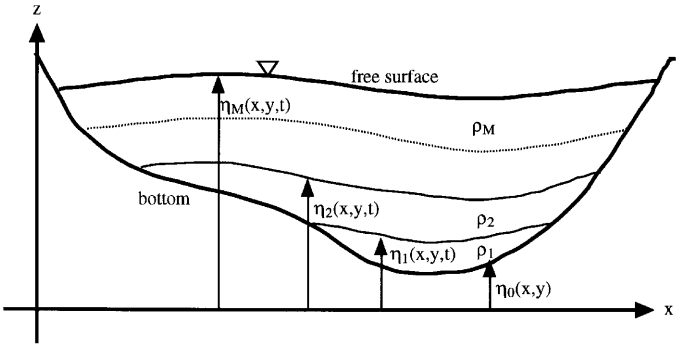

Figure 1. Isopycnal configuration

By setting $\rho_{M+1} = 0$, the governing equations can be written, after turbulent averaging and under the hydrostatic and Boussinesq approximations, in the form

$$\begin{aligned}
\frac{\partial u_k}{\partial t} + u_k \frac{\partial u_k}{\partial x} + v_k \frac{\partial u_k}{\partial y} &= -g \frac{\partial}{\partial x}\left(\sum_{m=k}^{M} \frac{\rho_m - \rho_{m+1}}{\rho_0} \eta_m \right) + v^{\mathrm{h}} \left(\frac{\partial^2 u_k}{\partial x^2} + \frac{\partial^2 u_k}{\partial y^2} \right) + \frac{\tau^x_{k+1/2} - \tau^x_{k-1/2}}{\eta_k - \eta_{k-1}}, \\
\frac{\partial v_k}{\partial t} + u_k \frac{\partial v_k}{\partial x} + v_k \frac{\partial v_k}{\partial y} &= -g \frac{\partial}{\partial y}\left(\sum_{m=k}^{M} \frac{\rho_m - \rho_{m+1}}{\rho_0} \eta_m \right) + v^{\mathrm{h}} \left(\frac{\partial^2 v_k}{\partial x^2} + \frac{\partial^2 v_k}{\partial y^2} \right) + \frac{\tau^y_{k+1/2} - \tau^y_{k-1/2}}{\eta_k - \eta_{k-1}},
\end{aligned} \tag{1}$$

where $u_k(x, y, t)$ and $v_k(x, y, t)$ are the horizontal, layer-averaged velocity components in the x- and y-direction respectively of the kth isopycnal layer ($k = 1, 2, \ldots, M$), t is the time, g is the gravitational acceleration, v^{h} is the horizontal eddy viscosity coefficient and $\tau^x_{k+1/2}$ and $\tau^y_{k+1/2}$ represent the shear stress between layers in the x- and y-direction, respectively.

The continuity equations, expressing the principle of conservation of mass, for each layer are given by

$$\frac{\partial \eta_k}{\partial t} + \frac{\partial}{\partial x}\left(\sum_{m=1}^{k} (\eta_m - \eta_{m-1}) u_m \right) + \frac{\partial}{\partial y}\left(\sum_{m=1}^{k} (\eta_m - \eta_{m-1}) v_m \right) = 0. \tag{2}$$

The boundary conditions at the free surface are specified by prescribing the wind stresses $\tau^x_{M+1/2}$ and $\tau^y_{M+1/2}$ as

$$\tau^x_{M+1/2} = \gamma_{\mathrm{T}}(u_{\mathrm{a}} - u_M), \qquad \tau^y_{M+1/2} = \gamma_{\mathrm{T}}(v_{\mathrm{a}} - v_M), \tag{3}$$

where γ_{T} is a non-negative wind stress coefficient and u_{a} and v_{a} are the prescribed wind velocity components in the x- and y-direction respectively. At the sediment–water interface the bottom friction is specified by

$$\tau^x_{1/2} = \gamma_{\mathrm{B}} u_1, \qquad \tau^y_{1/2} = \gamma_{\mathrm{B}} v_1, \tag{4}$$

where γ_{B} is a non-negative bottom friction coefficient. Typically, γ_{B} can be given by the Manning–Chezy formula or by fitting it to a turbulent boundary layer. Finally, the shear stress between layers is taken to be

$$\tau^x_{k+1/2} = 2v^{\mathrm{v}} \frac{u_{k+1} - u_k}{\eta_{k+1} - \eta_{k-1}}, \qquad \tau^y_{k+1/2} = 2v^{\mathrm{v}} \frac{v_{k+1} - v_k}{\eta_{k+1} - \eta_{k-1}}, \qquad k = 1, 2, \ldots, M-1, \tag{5}$$

where ν^{v} is a vertical eddy viscosity coefficient. This coefficient can be determined from an appropriate turbulence closure model, which is beyond the scope of the present investigation. Here it will only be assumed that ν^{v} is a prescribed non-negative function of space and time.

3. NUMERICAL APPROXIMATION

For stably stratified flows a numerical model in an isopycnal co-ordinate system is more attractive than models in either Cartesian (x, y, z) co-ordinates or σ-co-ordinates which are based on geometrical rather than physical considerations. Consequently, various numerical schemes for equations (1) and (2) have been studied and applied by several authors (see e.g. References 6–10).

In order to obtain an efficient numerical method whose stability is independent of the internal and free surface gravity wave speeds, a semi-implicit scheme is derived. The gradient of surface elevations in the horizontal momentum equations (1) and the velocity in the free surface equations (2) are discretized implicitly by the θ-method. Moreover, for stability the vertical viscosity terms (3)–(5) will be discretized implicitly.

The physical domain is subdivided into $N_x N_y$ rectangular cells of length Δx and width Δy, respectively. Each cell is numbered at its centre with indices i and j. The discrete velocities u_k are then defined at half-integer i and integer j; v_k are defined at integer i and half-integer j. Finally, η_k are defined at integer i, j.

A semi-implicit discretization for the momentum equations (1) takes the form

$$u^{n+1}_{i+1/2,j,k} = Fu^{n}_{i+1/2,j,k} - g\frac{\Delta t}{\Delta x}\sum_{m=k}^{M}\frac{\rho_m - \rho_{m+1}}{\rho_0}[\theta(\eta^{n+1}_{i+1,j,m} - \eta^{n+1}_{i,j,m}) + (1-\theta)(\eta^{n}_{i+1,j,m} - \eta^{n}_{i,j,m})]$$
$$+ \Delta t\frac{\nu^{\mathrm{v}}_{k+1/2}(u^{n+1}_{i+1/2,j,k+1} - u^{n+1}_{i+1/2,j,k})/\Delta\eta^{n}_{i+1/2,j,k+1/2} - \nu^{\mathrm{v}}_{k-1/2}(u^{n+1}_{i+1/2,j,k} - u^{n+1}_{i+1/2,j,k-1})/\Delta\eta^{n}_{i+1/2,j,k-1/2}}{\Delta\eta^{n}_{i+1/2,j,k}}, \tag{6}$$

$$v^{n+1}_{i,j+1/2,k} = Fv^{n}_{i,j+1/2,k} - g\frac{\Delta t}{\Delta y}\sum_{m=k}^{M}\frac{\rho_m - \rho_{m+1}}{\rho_0}[\theta(\eta^{n+1}_{i,j+1,m} - \eta^{n+1}_{i,j,m}) + (1-\theta)(\eta^{n}_{i,j+1,m} - \eta^{n}_{i,j,m})]$$
$$+ \Delta t\frac{\nu^{\mathrm{v}}_{k+1/2}(v^{n+1}_{i,j+1/2,k+1} - v^{n+1}_{i,j+1/2,k})/\Delta\eta^{n}_{i,j+1/2,k+1/2} - \nu^{\mathrm{v}}_{k-1/2}(v^{n+1}_{i,j+1/2,k} - v^{n+1}_{i,j+1/2,k-1})/\Delta\eta^{n}_{i,j+1/2,k-1/2}}{\Delta\eta^{n}_{i,j+1/2,k}}, \tag{7}$$

where $\Delta\eta_k = \eta_k - \eta_{k\text{-}1}$ denotes the layer thickness which also depends on the spatial location and on the time. $\Delta\eta_k$ is allowed to vanish in order to account for variable geometries and for the wetting and drying of isopycnal layers. Of course, the corresponding momentum equation (6) or (7) is not defined at a grid point characterized by $\Delta\eta_k = 0$ and accordingly the velocity value at this point is not relevant. Equations (6) and (7) also include the implicit discretizations of the boundary conditions (3) and (4) at the sediment–water interface and at the free surface for $k = 1$ and $k = M$ respectively. Finally, F denotes a finite difference operator corresponding to the explicit discretization of the convective and horizontal viscosity terms. A particular form for F can be chosen in a variety of ways; for example, a simple space-centred discretization can be used for the convective terms when a sufficiently large horizontal viscosity is being used. Alternatively, the upwind discretization does not require any physical viscosity, but large, and often unrealistic, numerical viscosity is produced by this

choice. A more convenient formulation of F, from both the stability and the accuracy point of view, results from use of an explicit Eulerian–Lagrangian discretization. In this case F is defined as

$$Fu^n_{i+1/2,j,k} = u^n_{i+1/2-a,j-b,k} + \nu^{\mathrm{h}} \frac{\Delta t}{\Delta x^2}(u^n_{i+3/2-a,j-b,k} - 2u^n_{i+1/2-a,j-b,k} + u^n_{i-1/2-a,j-b,k}) + \nu^{\mathrm{h}} \frac{\Delta t}{\Delta y^2}(u^n_{i+1/2-a,j+1-b,k} - 2u^n_{i+1/2-a,j-b,k} + u^n_{i+1/2-a,j-1-b,k}), \tag{8}$$

$$Fv^n_{i,j+1/2,k} = v^n_{i-a,j+1/2-b,k} + \nu^{\mathrm{h}} \frac{\Delta t}{\Delta x^2}(v^n_{i+1-a,j+1/2-b,k} - 2v^n_{i-a,j+1/2-b,k} + v^n_{i-1-a,j+1/2-b,k}) + \nu^{\mathrm{h}} \frac{\Delta t}{\Delta y^2}(v^n_{i-a,j+3/2-b,k} - 2v^n_{i-a,j+1/2-b,k} + v^n_{i-a,j-1/2-b,k}), \tag{9}$$

where a and b denote the Lagrangian displacement caused by the convective terms.[1]

For each i, j and for any choice used for F, equations (6) and (7) constitute a set of linear tridiagonal systems which, however, are coupled to the unknown water surface elevations η^{n+1}. In order to determine $\eta^{n+1}_{i,j,k}$, and for numerical stability, the new velocity field is required to satisfy the discrete analogue of the free surface equations (2):

$$\begin{aligned}\eta^{n+1}_{i,j,k} = \eta^n_{i,j,k} &- \theta \frac{\Delta t}{\Delta x}\left(\sum_{m=1}^{k} \Delta\eta^n_{i+1/2,j,m} u^{n+1}_{i+1/2,j,m} - \sum_{m=1}^{k} \Delta\eta^n_{i-1/2,j,m} u^{n+1}_{i-1/2,j,m})\right) \\ &- \theta \frac{\Delta t}{\Delta y}\left(\sum_{m=1}^{k} \Delta\eta^n_{i,j+1/2,m} v^{n+1}_{i,j+1/2,m} - \sum_{m=1}^{k} \Delta\eta^n_{i,j-1/2,m} v^{n+1}_{i,j-1/2,m}\right) \\ &- (1-\theta)\frac{\Delta t}{\Delta x}\left(\sum_{m=1}^{k} \Delta\eta^n_{i+1/2,j,m} u^n_{i+1/2,j,m} - \sum_{m=1}^{k} \Delta\eta^n_{i-1/2,j,m} u^n_{i-1/2,j,m}\right) \\ &- (1-\theta)\frac{\Delta t}{\Delta y}\left(\sum_{m=1}^{k} \Delta\eta^n_{i,j+1/2,m} v^n_{i,j+1/2,m} - \sum_{m=1}^{k} \Delta\eta^n_{i,j-1/2,m} v^n_{i,j-1/2,m}\right).\end{aligned} \tag{10}$$

Equations (6), (7) and (10) now form a linear system of $3MN_xN_y$ equations with unknowns $u^{n+1}_{i+1/2,j,k}$, $v^{n+1}_{i,j+1/2,k}$ and $\eta^{n+1}_{i,j,k}$.

4. SOLUTION ALGORITHM

For computational convenience, since a system of $3MN_xN_y$ equations can be quite large even for modest values of N_x, N_y and M, this system is first reduced to a smaller, block pentadiagonal system of only MN_xN_y equations in which $\eta^{n+1}_{i,j,k}$ are the only unknowns. Specifically, upon multiplication by $\Delta\eta^n_{i+1/2,j,k}$ and $\Delta\eta^n_{i,j+1/2,k}$, equations (6), (7) and (10) are first written in matrix notation as

$$\mathbf{A}^n_{i+1/2,j}\mathbf{U}^{n+1}_{i+1/2,j} = \mathbf{G}^n_{i+1/2,j} - g\frac{\theta\Delta t}{\rho_0\Delta x}\mathbf{S}^n_{i+1/2,j}\mathbf{R}(\boldsymbol{\eta}^{n+1}_{i+1,j} - \boldsymbol{\eta}^{n+1}_{i,j}), \tag{11}$$

$$\mathbf{A}^n_{i,j+1/2}\mathbf{V}^{n+1}_{i,j+1/2} = \mathbf{G}^n_{i,j+1/2} - g\frac{\theta\Delta t}{\rho_0\Delta y}\mathbf{S}^n_{i,j+1/2}\mathbf{R}(\boldsymbol{\eta}^{n+1}_{i,j+1} - \boldsymbol{\eta}^{n+1}_{i,j}), \tag{12}$$

$$\begin{aligned}\boldsymbol{\eta}^{n+1}_{i,j} = \boldsymbol{\delta}^n_{i,j} &- \theta\frac{\Delta t}{\Delta x}[(\mathbf{S}^n_{i+1/2,j})^{\mathrm{T}}\mathbf{U}^{n+1}_{i+1/2,j} - (\mathbf{S}^n_{i-1/2,j})^{\mathrm{T}}\mathbf{U}^{n+1}_{i-1/2,j}] \\ &- \theta\frac{\Delta t}{\Delta y}[(\mathbf{S}^n_{i,j+1/2})^{\mathrm{T}}\mathbf{V}^{n+1}_{i,j+1/2} - (\mathbf{S}^n_{i,j-1/2})^{\mathrm{T}}\mathbf{V}^{n+1}_{i,j-1/2}],\end{aligned} \tag{13}$$

where $\mathbf{G}^n_{i+1/2,j}$, $\mathbf{G}^n_{i,j+1/2}$ and $\boldsymbol{\delta}^n_{i,j}$ are vectors containing all the explicit terms in equations (6), (7) and (10) respectively, while $\mathbf{U}$, $\mathbf{V}$, $\boldsymbol{\eta}$, $\mathbf{S}$, $\mathbf{R}$ and $\mathbf{A}$ are defined as

$$\mathbf{U}^{n+1}_{i+1/2,j}=\begin{bmatrix} u^{n+1}_{i+1/2,j,M}\\ u^{n+1}_{i+1/2,j,M-1}\\ u^{n+1}_{i+1/2,j,M-2}\\ \vdots\\ u^{n+1}_{i+1/2,j,1}\end{bmatrix},\qquad \mathbf{V}^{n+1}_{i,j+1/2}=\begin{bmatrix} v^{n+1}_{i,j+1/2,M}\\ v^{n+1}_{i,j+1/2,M-1}\\ v^{n+1}_{i,j+1/2,M-2}\\ \vdots\\ v^{n+1}_{i,j+1/2,1}\end{bmatrix},\qquad \boldsymbol{\eta}^{n+1}_{i,j}=\begin{bmatrix} \eta^{n+1}_{i,j,M}\\ \eta^{n+1}_{i,j,M-1}\\ \eta^{n+1}_{i,j,M-2}\\ \vdots\\ \eta^{n+1}_{i,j,1}\end{bmatrix},$$

$$\mathbf{S}=\begin{bmatrix} \Delta\eta_M & & & & \mathbf{0}\\ \Delta\eta_{M-1} & \Delta\eta_{M-1} & & & \\ \Delta\eta_{M-2} & \Delta\eta_{M-2} & \Delta\eta_{M-2} & & \\ \cdot & \cdot & \cdot & \cdots & \\ \Delta\eta_1 & \Delta\eta_1 & \Delta\eta_1 & \cdots & \Delta\eta_1\end{bmatrix},$$

$$\mathbf{R}=\begin{bmatrix} \rho_M-\rho_{M+1} & & & & & \mathbf{0}\\ & \rho_{M-1}-\rho_M & & & & \\ & & \rho_{M-2}-\rho_{M-1} & & & \\ & & & \ddots & & \\ \mathbf{0} & & & & & \rho_1-\rho_2\end{bmatrix},$$

$$\mathbf{A}=\begin{bmatrix} \Delta\eta_M+\dfrac{v^{\mathrm{v}}_{M-1/2}\Delta t}{\Delta\eta_{M-1/2}}+\gamma_{\mathrm{T}}\Delta t & -\dfrac{v^{\mathrm{v}}_{M-1/2}\Delta t}{\Delta\eta_{M-1/2}} & & & \mathbf{0}\\ -\dfrac{v^{\mathrm{v}}_{M-1/2}\Delta t}{\Delta\eta_{M-1/2}} & \Delta\eta_{M-1}+\dfrac{v^{\mathrm{v}}_{M-1/2}\Delta t}{\Delta\eta_{M-1/2}}+\dfrac{v^{\mathrm{v}}_{M-3/2}\Delta t}{\Delta\eta_{M-3/2}} & -\dfrac{v^{\mathrm{v}}_{M-3/2}\Delta t}{\Delta\eta_{M-3/2}} & & \\ & \cdot & \cdot & \cdot & \\ & & \cdot & \cdot & \\ \mathbf{0} & & & -\dfrac{v^{\mathrm{v}}_{3/2}\Delta t}{\Delta\eta_{3/2}} & \Delta\eta_1+\dfrac{v^{\mathrm{v}}_{3/2}\Delta t}{\Delta\eta_{3/2}}+\gamma_{\mathrm{B}}\Delta t\end{bmatrix}.$$

Then formal substitution of the expressions for $\mathbf{U}^{n+1}_{i+1/2,j}$ and $\mathbf{V}^{n+1}_{i,j+1/2}$ from (11) and (12) into (13) yields

$$\begin{aligned}\mathbf{R}^{-1}\tilde{\boldsymbol{\eta}}^{n+1}_{i,j}&-g\theta^2\frac{\Delta t^2}{\rho_0\Delta x^2}\{[\mathbf{S}^{\mathrm{T}}\mathbf{A}^{-1}\mathbf{S}]^n_{i+1/2,j}(\tilde{\boldsymbol{\eta}}^{n+1}_{i+1,j}-\tilde{\boldsymbol{\eta}}^{n+1}_{i,j})-[\mathbf{S}^{\mathrm{T}}\mathbf{A}^{-1}\mathbf{S}]^n_{i-1/2,j}(\tilde{\boldsymbol{\eta}}^{n+1}_{i,j}-\tilde{\boldsymbol{\eta}}^{n+1}_{i-1,j})\}\\ &-g\theta^2\frac{\Delta t^2}{\rho_0\Delta y^2}\{[\mathbf{S}^{\mathrm{T}}\mathbf{A}^{-1}\mathbf{S}]^n_{i,j+1/2}(\tilde{\boldsymbol{\eta}}^{n+1}_{i,j+1}-\tilde{\boldsymbol{\eta}}^{n+1}_{i,j})-[\mathbf{S}^{\mathrm{T}}\mathbf{A}^{-1}\mathbf{S}]^n_{i,j-1/2}(\tilde{\boldsymbol{\eta}}^{n+1}_{i,j}-\tilde{\boldsymbol{\eta}}^{n+1}_{i,j-1})\}\\ =\boldsymbol{\delta}^n_{i,j}&-\theta\frac{\Delta t}{\Delta x}\{[\mathbf{S}^{\mathrm{T}}\mathbf{A}^{-1}\mathbf{G}]^n_{i+1/2,j}-[\mathbf{S}^{\mathrm{T}}\mathbf{A}^{-1}\mathbf{G}]^n_{i-1/2,j}\}-\theta\frac{\Delta t}{\Delta y}\{[\mathbf{S}^{\mathrm{T}}\mathbf{A}^{-1}\mathbf{G}]^n_{i,j+1/2}-[\mathbf{S}^{\mathrm{T}}\mathbf{A}^{-1}\mathbf{G}]^n_{i,j-1/2}\},\end{aligned}\tag{14}$$

where $\tilde{\boldsymbol{\eta}} = \mathbf{R}\boldsymbol{\eta}$. Since the matrix $\mathbf{A}$ is an M-matrix (see e.g. Reference 11, Chap. 15), $\mathbf{A}^{-1}$ has non-negative elements everywhere. Therefore the matrix $\mathbf{S}^{\mathrm{T}}\mathbf{A}^{-1}\mathbf{S}$ is also symmetric and non- negative. Hence equations (14) constitute a block pentadiagonal system of equations for $\tilde{\boldsymbol{\eta}}_{i,j}^{n+1}$ which is symmetric and positive definite. Thus it has a unique solution which can be efficiently determined by a preconditioned conjugate gradient method. Once the new locations of the density interfaces have been determined, equations (11) and (12) are used to evaluate the new velocities $\mathbf{U}_{i+1/2,j}^{n+1}$ and $\mathbf{V}_{i,j+1/2}^{n+1}$ throughout the flow domain.

5. STABILITY ANALYSIS

A rigorous stability analysis of a non-linear numerical model is quite complex and not always possible. In this section the stability of the semi-implicit finite difference method (11)–(13) will be analysed by using the von Neumann method under the simplifying assumptions that the governing differential equations (1) and (2) are linear, with constant coefficients and defined on an infinite horizontal domain, or with periodic boundary conditions on a finite domain. Additionally, the layer thickness $\Delta\eta$ and the density differences $\Delta\rho$ are assumed to be constant. Thus, by neglecting the non-linear convective terms and the wind speed and by assuming that γ_{T}, γ_{B} and v^{v} in the matrix $\mathbf{A}$ are non-negative constants, the difference equations (11)–(13) reduce to

$$\mathbf{A}\mathbf{U}_{i+1/2,j}^{n+1}+\theta r\frac{\Delta t}{\Delta x}\mathbf{S}(\boldsymbol{\eta}_{i+1,j}^{n+1}-\boldsymbol{\eta}_{i,j}^{n+1}) = \Delta\eta\mathbf{F}\mathbf{U}_{i+1/2,j}^{n}-(1-\theta)r\frac{\Delta t}{\Delta x}\mathbf{S}(\boldsymbol{\eta}_{i+1,j}^{n}-\boldsymbol{\eta}_{i,j}^{n}), \tag{15}$$

$$\mathbf{A}\mathbf{V}_{i,j+1/2}^{n+1}+\theta r\frac{\Delta t}{\Delta y}\mathbf{S}(\boldsymbol{\eta}_{i,j+1}^{n+1}-\boldsymbol{\eta}_{i,j}^{n+1}) = \Delta\eta\mathbf{F}\mathbf{V}_{i,j+1/2}^{n}-(1-\theta)r\frac{\Delta t}{\Delta y}\mathbf{S}(\boldsymbol{\eta}_{i,j+1}^{n}-\boldsymbol{\eta}_{i,j}^{n}), \tag{16}$$

$$\begin{aligned}\boldsymbol{\eta}_{i,j}^{n+1}+\theta\frac{\Delta t}{\Delta x}(\mathbf{S}^{\mathrm{T}}\mathbf{U}_{i+1/2,j}^{n+1}-\mathbf{S}^{\mathrm{T}}\mathbf{U}_{i-1/2,j}^{n+1})+\theta\frac{\Delta t}{\Delta y}(\mathbf{S}^{\mathrm{T}}\mathbf{V}_{i,j+1/2}^{n+1}-\mathbf{S}^{\mathrm{T}}\mathbf{V}_{i,j-1/2}^{n+1})\\ =\boldsymbol{\eta}_{i,j}^{n}-(1-\theta)\frac{\Delta t}{\Delta x}(\mathbf{S}^{\mathrm{T}}\mathbf{U}_{i+1/2,j}^{n}-\mathbf{S}^{\mathrm{T}}\mathbf{U}_{i-1/2,j}^{n})-(1-\theta)\frac{\Delta t}{\Delta y}(\mathbf{S}^{\mathrm{T}}\mathbf{V}_{i,j+1/2}^{n}-\mathbf{S}^{\mathrm{T}}\mathbf{V}_{i,j-1/2}^{n}),\end{aligned} \tag{17}$$

where $\mathbf{F}\mathbf{U}_{i+1/2,j}^{n}$ and $\mathbf{F}\mathbf{V}_{i,j+1/2}^{n}$ are the explicit finite difference discretizations of the horizontal eddy viscosity terms and r is the reduced gravity $r = g\Delta\rho/\rho_0$.

Theorem

The semi-implicit finite difference scheme (15)–(17) is stable in the von Neumann sense if $\frac{1}{2} \leqslant \theta \leqslant 1$ and if the time step Δt satisfies the inequality

$$\Delta t \leqslant \left[2v^{\mathrm{h}}\left(\frac{1}{\Delta x^2}+\frac{1}{\Delta y^2}\right)\right]^{-1}. \tag{18}$$

Proof. By replacing $\mathbf{U}_{i+1/2,j}^{n}$, $\mathbf{V}_{i,j+1/2}^{n}$ and $\boldsymbol{\eta}_{i,j}^{n}$ in (15)–(17) with the corresponding Fourier components $\hat{\mathbf{U}}^{n}\mathrm{e}^{\mathrm{i}[(i+1/2)\alpha+j\beta]}$, $\hat{\mathbf{V}}^{n}\mathrm{e}^{\mathrm{i}[i\alpha+(j+1/2)\beta]}$ and $\hat{\boldsymbol{\eta}}^{n}\mathrm{e}^{\mathrm{i}(i\alpha+j\beta)}$, after some simplifications, (15)–(17) become

$$\mathbf{A}\hat{\mathbf{U}}^{n+1}+\mathrm{i}\theta pr\mathbf{S}\hat{\boldsymbol{\eta}}^{n+1} = f\Delta\eta\hat{\mathbf{U}}^{n}-\mathrm{i}(1-\theta)pr\mathbf{S}\hat{\boldsymbol{\eta}}^{n}, \tag{19}$$

$$\mathbf{A}\hat{\mathbf{V}}^{n+1}+\mathrm{i}\theta qr\mathbf{S}\hat{\boldsymbol{\eta}}^{n+1} = f\Delta\eta\hat{\mathbf{V}}^{n}-\mathrm{i}(1-\theta)qr\mathbf{S}\hat{\boldsymbol{\eta}}^{n}, \tag{20}$$

$$\hat{\boldsymbol{\eta}}^{n+1}+\mathrm{i}p\theta\mathbf{S}^{\mathrm{T}}\hat{\mathbf{U}}^{n+1}+\mathrm{i}q\theta\mathbf{S}^{\mathrm{T}}\hat{\mathbf{V}}^{n+1} = \hat{\boldsymbol{\eta}}^{n}-\mathrm{i}p(1-\theta)\mathbf{S}^{\mathrm{T}}\hat{\mathbf{U}}^{n}+\mathrm{i}q(1-\theta)\mathbf{S}^{\mathrm{T}}\hat{\mathbf{V}}^{n}, \tag{21}$$

where $\hat{\mathbf{U}}^n$, $\hat{\mathbf{V}}^n$ and $\hat{\boldsymbol{\eta}}^n$ are the amplitude functions of $\mathbf{U}$, $\mathbf{V}$ and $\boldsymbol{\eta}$ at time level t_n respectively, $\mathrm{i} = \sqrt{(-1)}$, α and β are the x- and y-phase angles respectively, $p = 2(\Delta t/\Delta x)\sin(\alpha/2)$, $q = 2(\Delta t/\Delta y)\sin(\beta/2)$ and the amplification factor of the explicit difference operator F is given by

$$f = 1 - 2v^{\mathrm{h}}\Delta t\left(\frac{1-\cos(\alpha)}{\Delta x^2} + \frac{1-\cos(\beta)}{\Delta y^2}\right). \tag{22}$$

Equations (19)–(21) can be written in a more compact matrix form as

$$\mathbf{P}\hat{\mathbf{W}}^{n+1} = \mathbf{Q}\hat{\mathbf{W}}^n, \tag{23}$$

where

$$\hat{\mathbf{W}}^n = \begin{bmatrix} \hat{\mathbf{U}}^n \\ \hat{\mathbf{V}}^n \\ \hat{\boldsymbol{\eta}}^n \end{bmatrix}, \qquad \mathbf{P} = \begin{bmatrix} \mathbf{A} & \mathbf{0} & \mathrm{i}p\theta r\mathbf{S} \\ \mathbf{0} & \mathbf{A} & \mathrm{i}q\theta r\mathbf{S} \\ \mathrm{i}p\theta\mathbf{S}^{\mathrm{T}} & \mathrm{i}q\theta\mathbf{S}^{\mathrm{T}} & \mathbf{I} \end{bmatrix},$$

$$\mathbf{Q} = \begin{bmatrix} f\Delta\eta\mathbf{I} & \mathbf{0} & -\mathrm{i}p(1-\theta)r\mathbf{S} \\ \mathbf{0} & f\Delta\eta\mathbf{I} & -\mathrm{i}q(1-\theta)r\mathbf{S} \\ -\mathrm{i}p(1-\theta)\mathbf{S}^{\mathrm{T}} & -\mathrm{i}q(1-\theta)\mathbf{S}^{\mathrm{T}} & \mathbf{I} \end{bmatrix},$$

with $\mathbf{I}$ being the identity matrix of order M. Thus the amplification matrix of the method is $\mathbf{G} = \mathbf{P}^{-1}\mathbf{Q}$ and a condition for stability is that the spectral radius of $\mathbf{G}$ does not exceed unity independently of α and β. The characteristic polynomial of the matrix $\mathbf{G}$ is $\det(\mathbf{Q} - \lambda\mathbf{P}) = 0$, i.e.

$$\det(\mathbf{Q} - \lambda\mathbf{P}) = \det\begin{bmatrix} f\Delta\eta\mathbf{I} - \lambda\mathbf{A} & \mathbf{0} & -\mathrm{i}pr\omega\mathbf{S} \\ \mathbf{0} & f\Delta\eta\mathbf{I} - \lambda\mathbf{A} & -\mathrm{i}qr\omega\mathbf{S} \\ -\mathrm{i}p\omega\mathbf{S}^{\mathrm{T}} & -\mathrm{i}q\omega\mathbf{S}^{\mathrm{T}} & (1-\lambda)\mathbf{I} \end{bmatrix} = 0, \tag{24}$$

where $\omega = 1 - \theta + \lambda\theta$. Next to be shown is that equation (24) cannot be satisfied by any complex number λ when $|\lambda| > 1$. Assume that $|\lambda| > 1$ and consider the matrix $\mathbf{A}$ which is real, symmetric, strictly diagonally dominant and with positive eigenvalues $\lambda_k \geqslant \Delta\eta$. Note that when inequality (18) is satisfied, equation (22) implies $|f| \leqslant 1$. Therefore $|f\Delta\eta| < |\lambda\Delta\eta|$ and hence the matrix $f\Delta\eta\mathbf{I} - \lambda\mathbf{A}$ remains strictly diagonally dominant and invertible. Consider then

$$\mathbf{T} = \begin{bmatrix} \mathbf{I} & \mathbf{0} & \mathbf{0} \\ \mathbf{0} & \mathbf{I} & \mathbf{0} \\ \mathrm{i}p\omega\mathbf{S}^{\mathrm{T}}(f\Delta\eta\mathbf{I} - \lambda\mathbf{A})^{-1} & \mathrm{i}q\omega\mathbf{S}^{\mathrm{T}}(f\Delta\eta\mathbf{I} - \lambda\mathbf{A})^{-1} & \mathbf{I} \end{bmatrix},$$

so that

$$\det(\mathbf{Q} - \lambda\mathbf{P}) = \det(\mathbf{T})\det(\mathbf{Q} - \lambda\mathbf{P}) = \det[\mathbf{T}(\mathbf{Q} - \lambda\mathbf{P})]. \tag{25}$$

Thus equation (24) can also be written as

$$\det\begin{bmatrix} f\Delta\eta\mathbf{I} - \lambda\mathbf{A} & \mathbf{0} & -\mathrm{i}pr\omega\mathbf{S} \\ \mathbf{0} & f\Delta\eta\mathbf{I} - \lambda\mathbf{A} & -\mathrm{i}qr\omega\mathbf{S} \\ \mathbf{0} & \mathbf{0} & \mathbf{B} \end{bmatrix} = 0, \tag{26}$$

where

$$\mathbf{B} = r(p^2 + q^2)\omega^2\mathbf{S}^{\mathrm{T}}(f\Delta\eta\mathbf{I} - \lambda\mathbf{A})^{-1}\mathbf{S} + (1-\lambda)\mathbf{I}. \tag{27}$$

Since $\det(f\Delta\eta\mathbf{I} - \lambda\mathbf{A}) \neq 0$, it is only necessary to show that for $\frac{1}{2} \leqslant \theta \leqslant 1$ one has $\det(\mathbf{B}) \neq 0$. On the other hand, $f\Delta\eta\mathbf{I} - \lambda\mathbf{A}$ admits an $\mathbf{LDL}^{\mathrm{T}}$ decomposition, where $\mathbf{L}$ is a unitary lower triangular matrix

and **D** is a diagonal matrix with diagonal elements given by $f\Delta\eta - \lambda\lambda_k$. Consequently, the eigenvalues of **B** are given by

$$\lambda_B = \Delta\eta^2 \frac{r(p^2+q^2)\omega^2}{f\Delta\eta - \lambda\lambda_k} + 1 - \lambda. \tag{28}$$

Our objective now is to prove that for $\frac{1}{2} \leqslant \theta \leqslant 1$, $|\lambda| > 1$ and for every k one has $\lambda_B \neq 0$ or, equivalently,

$$d = \Delta\eta^2 r(p^2+q^2)\omega^2 + (1-\lambda)(f\Delta\eta - \lambda\lambda_k) \neq 0. \tag{29}$$

For this purpose let $\lambda = a + ib$, so that substitution of the expression for ω into (29), after simple manipulations, yields

$$\begin{aligned} d =& [\lambda_k + \theta^2\Delta\eta^2 r(p^2+q^2)](a^2-b^2) + f\Delta\eta + \Delta\eta^2 r(p^2+q^2)(1-\theta)^2 \\ & - [\lambda_k + f\Delta\eta - 2\theta(1-\theta)\Delta\eta^2 r(p^2+q^2)]a \\ & + i\{2\theta(1-\theta)r\Delta\eta^2(p^2+q^2)b - (\lambda_k + f\Delta\eta)b + 2[\lambda_k + \theta^2 r\Delta\eta^2(p^2+q^2)]ab\}. \end{aligned} \tag{30}$$

Consider first the case $b = 0$ and $|a| > 1$. In this case d is real and satisfies the inequality

$$\begin{aligned} d =& \lambda_k a^2 + r\Delta\eta^2(p^2+q^2)(1-\theta+\theta a)^2 + f\Delta\eta - (\lambda_k + f\Delta\eta)a \\ \geqslant& \lambda_k a^2 + f\Delta\eta - (\lambda_k + f\Delta\eta)a = (\lambda_k a + f\Delta\eta)(a-1) > 0. \end{aligned} \tag{31}$$

Consider next the case $b \neq 0$. In this case the imaginary part of d is non-zero unless a is given by

$$a = \frac{\lambda_k + f\Delta\eta - 2\theta(1-\theta)\Delta\eta^2 r(p^2+q^2)}{2[\lambda_k + \theta^2\Delta\eta^2 r(p^2+q^2)]}. \tag{32}$$

Should the imaginary part of d be zero, for $\frac{1}{2} \leqslant \theta \leqslant 1$, since $b^2 > 1 - a^2$, use of (32) yields the following inequality for the real part of d:

$$\begin{aligned} d <& [\lambda_k + \theta^2\Delta\eta^2 r(p^2+q^2)](2a^2-1) + f\Delta\eta + \Delta\eta^2 r(p^2+q^2)(1-\theta)^2 \\ & - [\lambda_k + f\Delta\eta - 2\theta(1-\theta)\Delta\eta^2 r(p^2+q^2)]a \\ =& f\Delta\eta + \Delta\eta^2 r(p^2+q^2)(1-\theta)^2 - [\lambda_k + \theta^2\Delta\eta^2 r(p^2+q^2)] \leqslant 0. \end{aligned} \tag{33}$$

Thus, when $\frac{1}{2} \leqslant \theta \leqslant 1$, under the stability restriction (18) the amplification matrix **G** does not have eigenvalues λ such that $|\lambda| > 1$. Therefore the spectral radius of **G** is no greater than unity and the scheme (15)–(17) is stable in the von Neumann sense.

Note that, as expected, the stability of the semi-implicit finite difference scheme (15)–(17) is independent of the celerity, bottom friction, wind stress and vertical viscosity. It does depend on the horizontal viscosity through the mild stability condition (18). This method becomes unconditionally stable when the horizontal viscosity terms are neglected.

The presence of non-linear convective terms may affect the stability of the method when they are discretized explicitly by standard schemes which use, for example, central or upwind differences. Use of Eulerian–Lagrangian methods as described in Reference 1 is always recommended because of their higher accuracy and because additional conditions for the stability are not required.

6. PROPERTIES OF METHOD

An important property of the present formulation is that each layer thickness $\Delta\eta_k$ is allowed to vanish. Thus each isopycnal layer k does not need to be present everywhere at all times. Of course, no flux will result through those cell faces characterized by $\Delta\eta_k = 0$ and flooding and drying of tidal flats are naturally included in this model.

Local and global conservation properties of both fluid volume and masses are assured by the conservative discretization scheme (10) chosen to approximate the free surface equations (2).

In the particular case of $M = 1$ the vertical spacing $\Delta\eta$ represents the total water depth H. Additionally in this case the vectors $\mathbf{U}$, $\mathbf{V}$, $\boldsymbol{\eta}$ and $\mathbf{G}$ and the matrices $\mathbf{S}$, $\mathbf{R}$ and $\mathbf{A}$ reduce to one element and the block pentadiagonal system (14) becomes a simple pentadiagonal system. Thus, in conclusion, one can easily verify that this algorithm reduces to a two-dimensional numerical method which is consistent with the two-dimensional, vertically integrated shallow water equations and which, for $\theta = 1$, yields the method described in Reference 1. This property of the algorithm leads to a computer code that can be used for both three-dimensional isopycnal problems as well as two-dimensional problems.

In applying this model, one should always make sure that all the assumptions made to guarantee the model applicability are satisfied. One such assumption is that the expected flow is stably stratified at all times. Thus physically unstable situations cannot be described by this model. In this respect, since in most geophysical flows the speed of internal waves is much smaller than the speed of free surface gravity waves, the internal flow may easily become supercritical and a smaller time step than given by inequality (18) may become necessary in order to obtain sufficient accuracy.

Although much better results are obtained by the present isopycnal model in terms of accuracy and computer performance, traditional three-dimensional models in Cartesian (x, y, z) co-ordinates retain the capability of describing the transport of passive components with greater vertical detail.

7. APPLICATIONS

In order to emphasize the more important aspects of the present formulation, we consider first the so-called 'lock exchange' problem which is a severe test case for traditional three-dimensional methods in (x, y, z) co-ordinates. A rectangular basin of width $L = 200$ m and depth $H = 0{\cdot}3$ m is initially filled with two fluids with different densities $\rho_1 = 1{\cdot}01$ g cm^{-3} and $\rho_2 = 1{\cdot}0$ g cm^{-3}, separated by a vertical dam located centrally in the basin (see Figure 2). The two fluids are assumed to be immiscible, so that once the dam is removed, the resulting flow is expected to keep a sharp interface of separation which evolves with two discontinuities moving in opposite directions. A natural choice for the vertical discretization in this case is $M = 2$, so that the initial values for η_0, η_1 and η_2 are taken to be $\eta_0 = -0{\cdot}3$ m, $\eta_2 = 0$ m, while $\eta_1 = 0$ m to the leftmost part of the basin and $\eta_1 = -0{\cdot}3$ m to the right. The initial velocities are zero and the discretization parameters are taken to be $\Delta x = 1$ m and $\Delta t = 10$ s. Figure 3 shows the resulting free surface configuration computed with the present algorithm at time $t = 1000$ s. The required CPU time for this example is of 22 s on a 100 MHz workstation. No sign of instability has been observed even though the bottom friction and horizontal and vertical viscosity terms have been neglected. For comparison this test case was reconsidered with a traditional three-dimensional model in Cartesian (x, y, z) co-ordinates as described in Reference 4, by including an equation for the density and with the addition of the baroclinic pressure terms in the momentum equations. The density equation was then discretized with a semi-implicit Eulerian–Lagrangian method, while the baroclinic terms have been discretized explicitly. Using the same Δx and Δt and with 30 vertical layers of constant $\Delta z = 0{\cdot}01$ m, the calculations were unstable, because the Courant–Friedrichs–Lewy condition on the internal wave speed was violated (see Figure 4). In

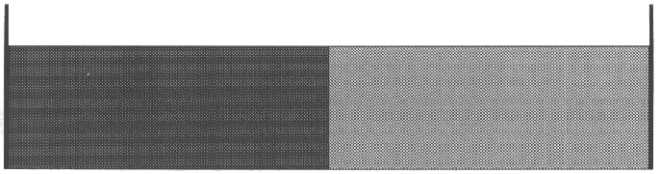

Figure 2. Initial state for lock exchange problem

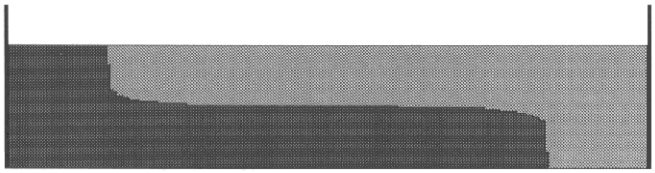

Figure 3. Numerical solution at $t = 1000$ s

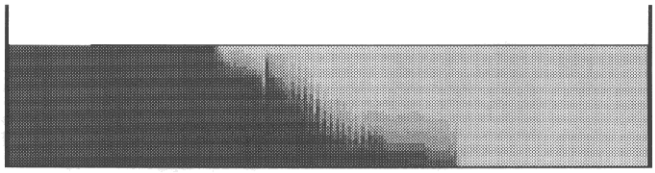

Figure 4. Unstable solution from an (x, y, z) model

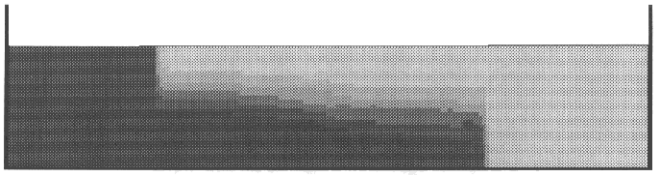

Figure 5. Stable solution obtained with $\Delta t = 2{\cdot}5$ s

order to comply with the CFL condition, the calculations were repeated with a smaller time step $\Delta t = 2{\cdot}5$ s. The resulting concentration field at time $t = 1000$ s was obtained in 174 s of CPU time and is shown in Figure 5. Not only do the results from the isopycnal model show a sharp fluid interface, but a substantial reduction in the computational cost results from usage of a simple two-layer isopycnal model.

Knowledge of lake dynamics is of great importance for the comprehension and management of water resources.[12] Most deep lakes in temperate zones present a classical thermocline structure during the summer period. Three-dimensional models in either Cartesian (x, y, z) co-ordinates or σ-co-ordinates would require an extremely large number of vertical grid points in order to resolve the sharp thermocline interface which separates the light, warm water floating on the heavy, cold water. For such a problem even a simple, two-layer isopycnal model may be much more accurate at a lower computational cost. This second example is aimed at showing the model applicability to the simulation of surface and internal waves in stratified lakes. The wind-driven circulation of Lake Garda has been considered for a typical summer situation. Lake Garda, the largest Italian lake, covers an area of 379 km^2 and has a perimeter of 185 km. In the northern part of the lake the water depth

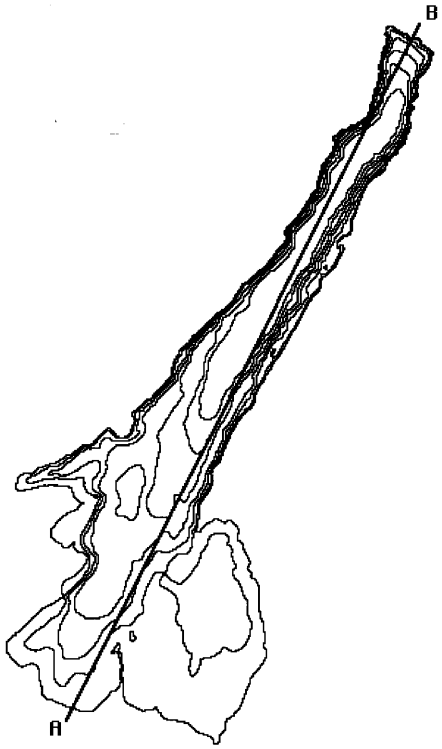

Figure 6. Bathymetry of Lake Garda

reaches 346 m (see Figure 6). The lake has been covered with a horizontal grid of $N_x = 330$ by $N_y = 515$ nodes equally spaced with $\Delta x = \Delta y = 100$ m. In order to represent the thermocline, a simple initial configuration of three flat isopycnal layers is considered with $\eta_1 = -30$ m, $\eta_2 = -20$ m and $\eta_3 = 0$ m separating fluids with densities $\rho_1 = 1{\cdot}002$ g cm^{-3}, $\rho_2 = 1{\cdot}001$ g cm^{-3} and $\rho_3 = 1{\cdot}0$ g cm^{-3} respectively (see Figure 7). Then a strong wind with constant speed $u_a = 10$ m s^{-1} u and $v_a = 20$ m s^{-1} was applied for the first 12 h of simulation. The resulting longitudinal isopycnal configurations along the section A–B at times $t = 12$, 36 and 120 h are shown in Figures 8–10 respectively. Specifically, Figure 8 shows the vanishing of the thicknesses of the top two layers as a

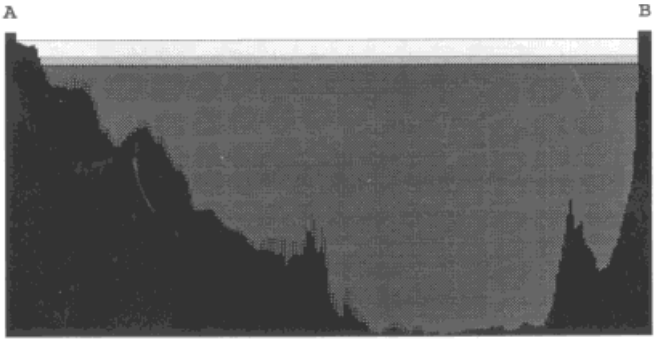

Figure 7. Initial conditions of steady thermocline

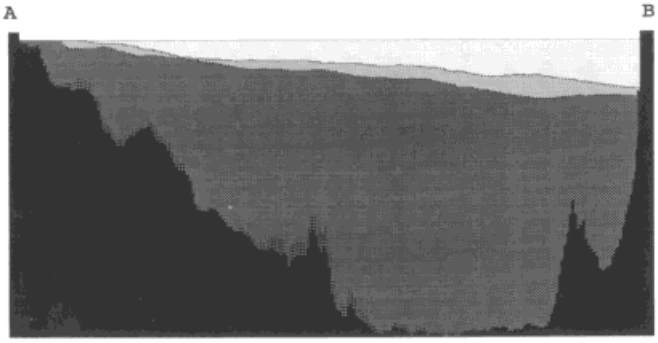

Figure 8. Wind-induced isopycnal layers at $t = 12$ h

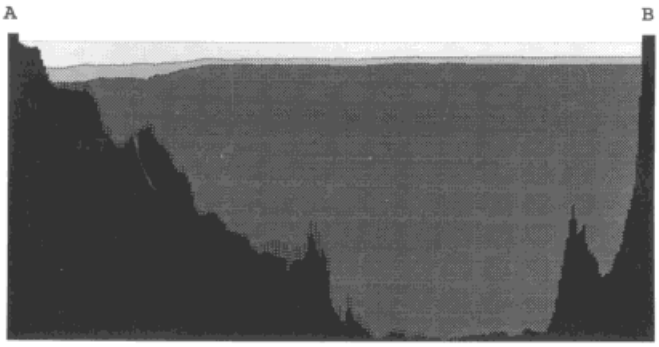

Figure 9. Resulting internal seiching generated at $t = 36$ h

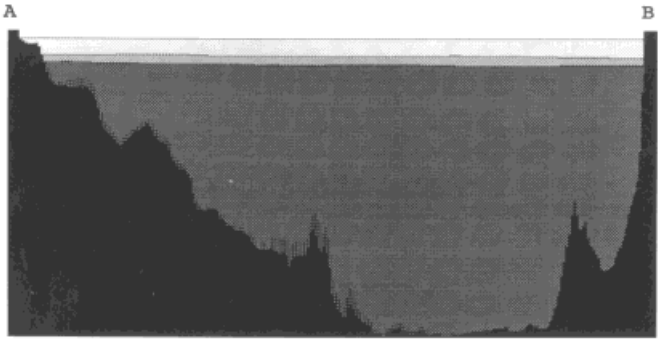

Figure 10. Almost steady state at $t = 120$ h

result of the strong upwelling in the southern part of the lake. Since the wind stops blowing at time $t = 12$ h, a lake-scale motion in the form of internal seiching is generated (see Figure 9). As time evolves without wind, the steady state configuration shown in Figure 7 is approached asymptotically. Figure 10 shows the residual internal waves computed at time $t = 120$ h. The free surface

displacement is too small to be shown in these figures. In this run the vertical eddy viscosity has been parametrized by a zero-order, flow-related and Richardson-number-dependent turbulence model derived under the assumption that the turbulence is in a state of local equilibrium.[13]

8. CONCLUSIONS

A semi-implicit finite difference method for solving the three-dimensional Reynolds-averaged Navier–Stokes equations in isopycnal (x, y, ρ) co-ordinates has been outlined. The implicit coupling between the momentum and free surface equations renders this scheme unconditionally stable with respect to the internal and surface wave speeds. Since in most geophysical applications the horizontal grid spacing is much larger than the layer thickness, the bottom friction and vertical shear terms have also been discretized implicitly in order to improve the numerical stability. Both the barotropic and baroclinic components of the hydrostatic pressure are determined implicitly by solving a block pentadiagonal linear system defined over the two-dimensional x–y domain. The layer-averaged horizontal velocities are then obtained as solutions of a large set of small tridiagonal linear systems. Two computational examples have been provided to show the model's ability to simulate baroclinic flows.

REFERENCES

1. V. Casulli, 'Semi-implicit finite difference methods for the two-dimensional shallow water equations', *J. Comput. Phys.*, **86**, 56–74 (1990).
2. V. Casulli and R. T. Cheng, 'Semi-implicit finite difference methods for three-dimensional shallow water flow', *Int. j. numer. methods fluids*, **15**, 629–648 (1992).
3. R. T. Cheng, V. Casulli and J. W. Gartner, 'Tidal, residual, intertidal mudflat (TRIM) model and its applications to San Francisco Bay, California', *Estuar., Coastal Shelf Sci.*, **36**, 235–280 (1993).
4. V. Casulli and E. Cattani, 'Stability, accuracy and efficiency of a semi-implicit method for three-dimensional shallow water flow', *Comput. Math. Appl.*, **27**, 99–112 (1994).
5. B. Cushman-Roisin, *Introduction to Geophysical Fluid Dynamics*, Prentice-Hall, Englewoods Cliffs, NJ, 1994.
6. R. Bleck and D. Boudra, 'Wind-driven spin-up in eddy-resolving ocean models formulated in isopycnic and isobaric coordinates', *J. Geophys. Res. (Oceans)*, **91**, 7611–7621 (1986).
7. J. M. de Kok, *Numerical Modeling of Transport Processes in Coastal Waters*, Ministry of Transport, Public Works and Water Management, RIKZ, The Hague, NL, 1994.
8. S.-K. Liu and J. J. Leendertse, 'Multidimensional numerical modeling of estuaries and coastal seas', in V. T. Chow (ed.), *Advances in Hydroscience*, Vol. II, Academic Press, NY, 1978, pp. 95–164.
9. J. M. Oberhuber, 'Simulation of the Atlantic circulation with a coupled sea ice–mixed layer–isopycnal general circulation model', *Max-Planck-Institut für Meteorologie*, *Report 59*, 1990.
10. T. J. Simons, 'Development of three-dimensional numerical models of the Great Lakes', *Scientific Ser. 12*, Canada Centre for Inland Waters, Burlington, On., 1973.
11. P. Lancaster and M. Tismenetsky, *The Theory of Matrices. Second Edition with Applications*, Academic, New York, 1985.
12. W. H. Graf, 'Waves on and in Lake of Geneva', *Proc. AIRH–IAHR Congr.*, Delft, NL, 1987, pp. 1–49.
13. W. Rodi, *Turbulence Models and Their Applications in Hydraulics*, 2nd edn, IAHR, Delft, NL, 1984.

